Interaction of NH($X\,^3\Sigma^-$) with He: Potential energy surface, bound states, and collisional Zeeman relaxation

H. Cybulski
Department of Chemistry, University of Warsaw, Pasteura 1, 02-093 Warszawa, Poland and Institute of Theoretical Chemistry, NSRIM, University of Nijmegen, Toernooiveld 1, 6525 ED Nijmegen, The Netherlands

R. V. Krems,[a] H. R. Sadeghpour, and A. Dalgarno
ITAMP, Harvard-Smithsonian Center for Astrophysics, 60 Garden Street, Cambridge, Massachusetts 02138

J. Kłos,[b] G. C. Groenenboom,[c] and A. van der Avoird[d]
Institute of Theoretical Chemistry, NSRIM, University of Nijmegen, Toernooiveld 1, 6525 ED Nijmegen, The Netherlands

D. Zgid
Department of Chemistry, University of Warsaw, Pasteura 1, 02-093 Warszawa, Poland

G. Chałasiński
Department of Chemistry, University of Warsaw, Pasteura 1, 02-093 Warszawa, Poland and Department of Chemistry, Oakland University, Rochester, Michigan 48309

(Received 17 August 2004; accepted 16 December 2004; published online 28 February 2005)

A detailed analysis of the He–NH($^3\Sigma^-$) van der Waals complex is presented. We discuss *ab initio* calculations of the potential energy surface and fitting procedures with relevance to cold collisions, and we present accurate calculations of bound energy levels of the triatomic complex as well as collisional properties of NH molecules in a buffer gas of ^{3}He. The influence of the external magnetic field used to trap the NH molecules and the effect of the atom–molecule interaction potential on the collisionally induced Zeeman relaxation are explored. It is shown that minute variations of the interaction potential due to different fitting procedures may alter the Zeeman relaxation rate at ultralow temperatures by as much as 50%. © *2005 American Institute of Physics*.
[DOI: 10.1063/1.1857473]

I. INTRODUCTION

Molecular physics has recently seen a revival due to the creation of ultracold molecules.[1] The research on ultracold molecules may lead to controlled chemistry, spectroscopy of unprecedented precision, and quantum computation. Several different techniques for producing ultracold molecules have been investigated with spectacular results.[2–16] The further development and extension of experimental techniques rest upon a close interaction with theory. Theoretical calculations in the cold and ultracold regimes necessitate extreme accuracy that can only be achieved through correspondence with observations. Subtle details of quantum chemistry techniques, fitting procedures for potential energy surfaces, and numerical analysis could significantly influence computation of collisional properties.

While it is known that the cross section for elastic scattering of molecules at ultracold temperatures may change from zero to infinity by slight variations of the intermolecular potential, the sensitivity of ultracold inelastic cross sections to the interaction potential remains an open question. Even if one applies the most advanced quantum chemistry methods with large basis sets to obtain accurate intermolecular potentials, fitting of the computed energy points by an analytical expression—necessary for calculations of molecular dynamics—introduces an uncertainty to the potential energy surface. A calculation of inelastic collision dynamics with two interaction potentials based on different fitting procedures provides an indication of the accuracy that can be achieved in inelastic scattering calculations at ultracold temperatures.

One of the most promising methods for the production of ultracold molecules relies on buffer-gas cooling.[15,16] Molecules are slowed down to temperatures near or less than 1 K by thermalization in a precooled buffer gas, usually ^{3}He, and captured in a magnetic trap with strong field gradients. The trapping efficiency depends critically on rate constants for elastic and inelastic collisions of the molecules with the buffer-gas atoms. The molecules are trapped in their low field–seeking state, which is the Zeeman level with the highest energy, and the efficiency of the buffer-gas loading is determined by the ratio of the rate constants for elastic scattering (cooling) and Zeeman relaxation (trap loss) in collisions with He atoms. The thermalization of the rotational levels of the molecules occurs at a rate which is usually comparable to the rate for cooling of the translational mo-

[a]Electronic mail: rkrems@cfa.harvard.edu
[b]Electronic mail: jakl@theochem.ru.nl
[c]Electronic mail: gerritg@theochem.ru.nl
[d]Electronic mail: avda@theochem.ru.nl

tion, and the majority of trapped molecules are in their lowest rotational state. It is therefore important to identify the mechanisms by which collisions with He atoms induce Zeeman transitions in rotationally ground-state molecules in order to predict which molecules are amenable to buffer-gas cooling. The papers of Volpi and Bohn,[17] Bohn,[18–20] and Avdeenkov and Bohn[21] are the only previous studies of magnetic transitions in atom–molecule and molecular collisions.

The buffer-gas loading method was used to produce the first trapped molecule CaH and experiments are in progress to trap another polar molecule NH.[15,22] The ground electronic state of CaH has $^2\Sigma^+$ symmetry, while that of NH has $^3\Sigma^-$ symmetry. We have recently demonstrated that Zeeman transitions in collision of rotationally ground-state $^2\Sigma$ and $^3\Sigma$ molecules with He atoms are induced by coupling between molecular rotational energy levels due to the anisotropy of the He–molecule interaction.[23–26] The Zeeman relaxation in $^2\Sigma$ molecules occurs through a three-step mechanism involving transitions to asymptotically closed rotationally excited levels and the action of the spin-rotation interaction in the excited states.[23] The Zeeman transitions in collision of $^3\Sigma$ molecules with He atoms are induced, on the other hand, by direct coupling due to the anisotropy of the atom–molecule interaction potential and the spin-spin interaction in the molecule.[24] The spin-rotation interaction is negligible in comparison.

In this work, we present an extensive discussion of our *ab initio* potential energy surface calculations, fitting procedures suitable for studies of molecular collisions at ultracold temperatures, bound states of the He–NH complex, and cross sections for elastic scattering and Zeeman relaxation over a wide range of collision energies and magnetic fields. We analyze the difference between the mechanisms of Zeeman relaxation in $^2\Sigma$ and $^3\Sigma$ molecules, and explore the sensitivity of the Zeeman relaxation cross sections to the interaction potential. To investigate the accuracy one can hope to achieve in *ab initio* dynamical calculations, we compute the Zeeman relaxation cross sections with two analytical fits of basically the same *ab initio* potential energy surface. Both fitting procedures employ large numbers of *ab initio* data points and analytical forms based on physical principles, and they are standard.

II. *AB INITIO* CALCULATIONS

The electronic potential energy surface for He–NH($X\ ^3\Sigma^-$) was computed using a supermolecular approach that defines the intermolecular interaction energy as

$$\Delta E_{AB}(R,\theta) = E_{AB}^{\mathrm{DB}}(R,\theta) - E_A^{\mathrm{DB}}(R,\theta) - E_B^{\mathrm{DB}}(R,\theta). \tag{1}$$

Using the counterpoise correction method of Boys and Bernardi[27] both the dimer and monomer energies were calculated in the dimer basis. The computations were performed with the MOLPRO 2000 program package.[28] The $X\ ^3\Sigma^-$ state of NH is odd under reflection in the plane containing the NH axis, and for nonlinear He–NH geometries the electronic ground state of the complex has A'' symmetry under reflection in the plane containing all the nuclei.

The geometry of the He–NH complex is described in Jacobi coordinates: the vector $\boldsymbol{r}$ joining the atoms in the diatomic molecule, the vector $\boldsymbol{R}$ joining the centers of mass of NH and He, and the angle θ between $\boldsymbol{R}$ and $\boldsymbol{r}$; $\theta=0°$ corresponds to the NH–He collinear configuration. The NH bond length was fixed at its equilibrium value of $r=1.0362$ Å.[29] The potential was calculated independently by two groups yielding two different sets of *ab initio* data. Calculations of potential I were performed for 18 values of R in the range from 3.0 to 15.0 bohrs (a_0) and 19 values of θ (steps of 10°) in the interval from 0° to 180°. Potential II was computed on a grid of 29 points in R and 30 points in θ chosen to coincide with the Gauss–Legendre quadrature points so that the integration over θ required to produce a Legendre expansion of the potential could be performed without interpolation.

Reference orbitals for spin-restricted coupled-cluster calculations with single, double, and noniterative triple excitations were obtained from spin-restricted Hartree–Fock calculations. The coupled-cluster calculations were performed in an all-electron approach. The basis consisted of augmented correlation-consistent quadruple zeta basis sets (denoted as aug-cc-pVQZ) on the NH molecule and on the He atom. This basis set was further augmented by a set of bond functions $[3s3p2d2f\ 1g]$ centered at the midpoint of the vector $\boldsymbol{R}$ to obtain a better description of the dispersion component of the interaction energy. These bond functions have the following exponents: *sp*: 0.9, 0.3, 0.1, *df*: 0.6, 0.2, and *g*: 0.3. Additional calculations with a quintuple zeta aug-cc-pV5Z basis reproduced well the interaction energy computed with the aug-cc-pVQZ basis. The minimum computed with this much larger basis is less than 0.5% deeper.

III. POTENTIAL ENERGY SURFACE

Collisions of molecules at low temperatures are determined by long-range interaction forces. An analytical form of the intermolecular potential suitable for studies of ultracold temperature dynamics should provide an adequate description of the long-range intermolecular potential. Particular care should be taken with the physical representation of the angular dependence of the potential energy at large atom–molecule separations.

An analytic fit to potential I was obtained by a three-step procedure similar to that described in Ref. 30. First, we fitted the *ab initio* points in the interval of R between $10a_0$ and $15a_0$ to a long-range expansion,

$$V_{\mathrm{LR}}(R,\theta) = \sum_{n=6}^{7} \sum_{\lambda=0}^{n-4} C_{n,\lambda} R^{-n} P_\lambda(\cos\ \theta), \tag{2}$$

P_λ being Legendre polynomials. Only even values of λ occur for $n=6$, and only odd values for $n=7$. The fit of the long-range coefficients $C_{n,\lambda}$ was obtained using a linear least squares method with a weighting function $w(R)=R^6$. Second, radial fits of the potential energy curves were generated for every value of the angle θ. The parameters $C_{6,0}$ and $C_{6,2}$ were fixed at the values obtained in the first step to ensure the correct long-range behavior. The *ab initio* points for each value of θ were fitted to Degli–Esposti–Werner[31] functions,

$$V(R) = G(R)\exp(-a_1R - a_2) - T(R)\sum_{n=6}^{10} C_nR^{-n} \tag{3}$$

with polynomials

$$G(R) = \sum_{j=0}^{8} g_jR^j \tag{4}$$

and a damping function

$$T(R) = \tfrac{1}{2}[1 + \tanh(1 + tR)]. \tag{5}$$

In this fit, we used the weighting function w_{SR} w_{LR} with the short-range part

$$w_{SR} = [\ln(e^{V/V_0} + e - 1)]^{-1} \tag{6}$$

and the long-range part

$$w_{LR} = \frac{1 + (R/R_0)^6}{V_0}, \tag{7}$$

where $V_0 = C_6R_0^{-6}$.[30] The parameter V_0 determines the distance at which the short-range factor of the weighting function effectively "switches on." We set it equal to $V_0 = 5|E_0|$, where E_0 is the most negative *ab initio* point, and chose $R_0 = 6.0a_0$. The parameters a_i, g_j, t, and C_n with $n > 6$ were optimized for each value of θ with the modified Levenberg–Marquardt algorithm from the MINPACK set of routines for nonlinear least squares fitting. The root mean square deviation of one-dimensional (1D) fits did not exceed 10^{-3} cm^{-1}. The error of the radial fit at short range was within 0.01%. The absolute error in the global minimum region for $R = 6.5a_0$ is 7.2×10^{-5} cm^{-1} and at $R = 15.0a_0$ it is 3×10^{-4} cm^{-1}. In the region of the van der Waals minimum, the relative error was 0.0004%, and at long range, it was smaller than 0.14%, the largest relative error for $R = 15.0a_0$.

Finally, using all of the 19 one-dimensional fits, we constructed the two-dimensional potential energy surface by expanding the potential in a series of Legendre polynomials $P_\lambda(\cos\theta)$,

$$V(R,\theta) = \sum_{\lambda=0}^{11} v_\lambda(R)P_\lambda(\cos\theta). \tag{8}$$

The coefficients $v_\lambda(R)$ for a given R were determined from a linear least squares fit to the data obtained from the previous 1D radial fits. The final error of the expansion in a series of 12 Legendre polynomials of the 19 angular points was about 0.8 cm^{-1} (or 0.01%) at short range ($R \approx 4.0a_0$). In the van der Waals minimum region at $R = 6.5a_0$, the absolute error of the expansion was about 8×10^{-4} cm^{-1} or 0.004%, and in the long range the relative error was 0.01%.

Potential II was directly expanded in a Legendre series with $\lambda_{max} = 11$; see Eq. (8). The potential was computed on a Gauss–Legendre quadrature grid for the angle θ and the expansion coefficients $v_\lambda(R)$ were obtained by numerical integration over θ, for each point of the radial grid. Next, they were fitted to the analytical expressions

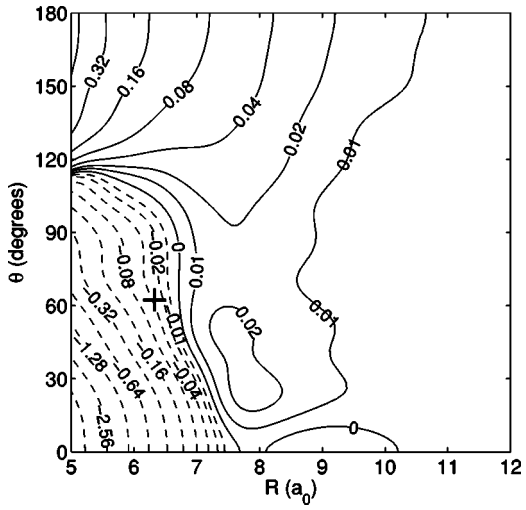

FIG. 1. Difference between the potentials: potential I minus potential II (cm^{-1}). The cross indicates the position of the minimum in potential I; see Fig. 2.

$$v_\lambda(R) = G_\lambda(R)\exp(-a_{\lambda,1}R - a_{\lambda,2}) - T_\lambda(R)\sum_{n=6}^{n_{max}} C_{n,\lambda}R^{-n}, \tag{9}$$

where the coefficients $g_{\lambda,j}$ in the polynomial $G_\lambda(R)$, of Eq. (4), and the parameter t_λ in the damping function $T_\lambda(R)$, of Eq. (5), are selected for each value of λ. For given λ the values of n in the long-range R^{-n} expansion are restricted by the condition that $n \geqslant \lambda + 4$ and that n must be even/odd for even/odd λ. The lowest five values of n permitted by these restrictions were included, which makes $n_{max} = 23$ for $\lambda = 11$. For the isotropic term with $\lambda = 0$ it was found that terms with $n > 8$ did not improve the fit, and the long-range expansion was limited to the R^{-6} and R^{-8} terms. In comparison with the fit of potential I [Eq. (3)], terms with higher n were retained in the asymptotic long-range form. The average error of the resulting representation of potential II is less than 0.04% and the maximum error of the analytical fit is 0.83%.

The main difference between the fitting procedures of the two potentials is the order of the radial and angular fitting and, consequently, in the truncation of the series of analytical fitting functions. Figure 1 displays the small differences of the potentials I and II. (Results presented in the preceding communication[25,26] were obtained using potential II.) Since we had available these two potentials computed and fitted independently by two groups, which may both be considered to be quite accurate, we used them to study the sensitivity of the elastic and inelastic collision cross sections at very low temperatures to subtle variations of the potential surface caused by differences in the fitting procedure and the different choice of the *ab initio* points.

A contour plot of potential surface I is shown in Fig. 2. The global minimum with energy −19.84 cm^{-1} is found for a skew T-shaped geometry with $R = 6.33a_0$ and $\theta = 62.3°$. Saddle points occur at both linear geometries. The lower saddle point with energy −16.58 cm^{-1} appears at $R = 7.20a_0$

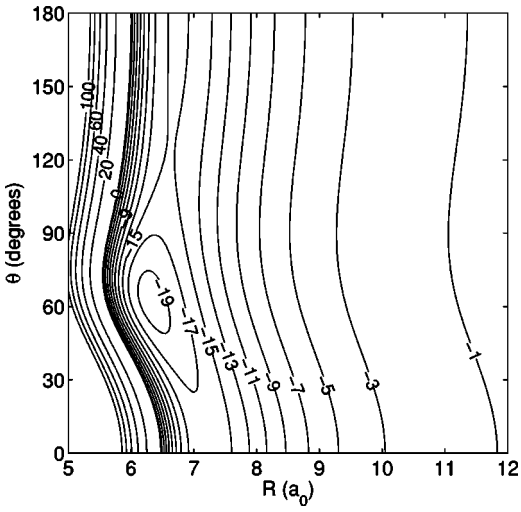

FIG. 2. Contour plot of the He–NH($X\ ^3\Sigma^-$) potential surface—potential I (in cm^{-1}). For a 3D plot of potential II, see Ref. 25.

when the He atom approaches the H atom, and the other saddle point with energy $-15.34\ cm^{-1}$ on the N side occurs at $R=6.74a_0$.

IV. BOUND STATE CALCULATIONS

To obtain the rovibrational energy levels of the ^{3}He–NH and ^{4}He–NH molecules with the $X\ ^3A''$ potential energy surface, we used the methodology described by Tennyson and Mettes[32] and by Jansen *et al.*[33] The He–NH Hamiltonian can be written in the space-fixed (SF) coordinate system as follows:

$$H=\frac{-\hbar^2}{2\mu R}\frac{\partial^2}{\partial R^2}R+\frac{L^2}{2\mu R^2}+b_{\mathrm{NH}}N^2+2\lambda_0(3S_\zeta^2-S^2)/3 + \gamma_0 \boldsymbol{N}\cdot\boldsymbol{S}+V(R,\theta), \tag{10}$$

where μ is the reduced mass of the complex, $\boldsymbol{N}$ is the rotational angular momentum of NH, and $\boldsymbol{L}$ is the angular momentum describing the rotation of the vector $\boldsymbol{R}$; $b_{\mathrm{NH}}=16.343\ cm^{-1}$ is the rotational constant of NH in its ground vibrational level;[34] $\lambda_0=0.920\ cm^{-1}$ and $\gamma_0=-0.055\ cm^{-1}$ are, respectively, the spin-spin and spin-rotation interaction constants for NH.[34] The operator S_ζ gives the component of the electronic spin $\boldsymbol{S}$ on the NH molecular axis; the expression for the spin-spin coupling term in SF coordinates is

$$2\lambda_0(3S_\zeta^2-S^2)/3=\frac{2}{3}\lambda_0\left[\frac{4\pi}{5}\right]^{1/2}\sqrt{6} \times\sum_q(-1)^q Y_{2,-q}(\hat{\boldsymbol{r}})[\boldsymbol{S}\otimes\boldsymbol{S}]_q^{(2)}, \tag{11}$$

where $\hat{\boldsymbol{r}}$ represents the polar angles that describe the direction of $\boldsymbol{r}$ in the SF frame. The second rank spherical tensor $[\boldsymbol{S}\otimes\boldsymbol{S}]^{(2)}$ is the tensorial product of $\boldsymbol{S}$ with itself.[35] The Legendre expansion in Eq. (8) of the potential $V(R,\theta)$ can be explicitly written in SF coordinates using the spherical harmonic addition theorem,[36]

$$P_\lambda(\cos\ \theta)=\left(\frac{4\pi}{2\lambda+1}\right)\sum_{m_\lambda}(-1)^{m_\lambda}Y_{\lambda,-m_\lambda}(\hat{\boldsymbol{R}})Y_{\lambda,m_\lambda}(\hat{\boldsymbol{r}}), \tag{12}$$

with $\hat{\boldsymbol{R}}$ representing the polar angles of $\boldsymbol{R}$ in the SF frame.

The total angular momentum of the diatomic molecule $\boldsymbol{j}=\boldsymbol{N}+\boldsymbol{S}$ is a good quantum number at $R=\infty$. The spin-spin and spin-rotation interactions are much smaller than the rotational constant b_{NH} so that the NH molecule is a Hund's case (b) system. This implies that N is approximately a good quantum number at $R=\infty$. The eigenvalues and eigenfunctions of the Hamiltonian H are determined variationally with the basis

$$\chi_q(R)|((NS)jL)JM_J\rangle, \tag{13}$$

where $\chi_q(R)$ are radial basis functions and $|((NS)jL)JM_J\rangle$ are the rotational and spin bases. The basis $|((NS)jL)JM_J\rangle$ is obtained by successive Clebsch–Gordan couplings: first the spherical harmonics $Y_{NM_N}(\hat{\boldsymbol{r}})$ are coupled with the spin functions τ_{SM_S}, then the resulting functions labeled with j and m_j are coupled with $Y_{LM_L}(\hat{\boldsymbol{R}})$ to obtain eigenfunctions of J^2 and J_z. The total angular momentum operator is $\boldsymbol{J}=\boldsymbol{j}+\boldsymbol{L}$ and J_z gives the z component of $\boldsymbol{J}$ in the SF frame. The conserved quantum numbers are J, its SF projection M_J, and the total parity $p=(-1)^{N+L+1}$. States with $N\leqslant N_{\max}=10$ were included in the basis set $|((NS)jL)JM_J\rangle$. The quantum numbers j and L take all values allowed by the triangular rule for coupling to a given value of J and parity p. For the radial basis $\chi_q(R)$ we used 25 Morse oscillator type functions.[37] The nonlinear parameters $R_e=11.50a_0$, $D_e=20.90\ cm^{-1}$, and $\omega_e=10.08\ cm^{-1}$ in this basis were optimized in calculations with a smaller basis. A grid of 40 points was used for the radial numerical integration.

To verify our results we repeated the computations of the rovibrational energy levels in a body-fixed (BF) basis using a parity-adapted Hund's case (a) representation for the NH monomer functions with $j_{\max}=8$. The radial basis in the BF program consisted of 25 contracted sinc–discrete variable representation functions[38,39] on a grid that ranges from $R=3.34a_0$ to $30a_0$ with step size $0.086a_0$. The R-dependent reference potential for the contraction was the isotropic potential, supplemented with a term linear in R. The isotropic potential has only one bound state and the linear term is added in order to localize the radial basis in the region of interest; its slope of $0.2mE_H/a_0$ was variationally optimized for the bound levels of the complex.

V. SCATTERING CALCULATIONS

The cross sections and rate constants for collisions of NH molecules with He atoms in a magnetic field were computed using the methodology described in detail by Krems and Dalgarno.[24] The interaction of the molecule with the magnetic field is added to the Hamiltonian of Eq. (10) in the form $g\mu_0\boldsymbol{B}\cdot\boldsymbol{S}$, where $g=2.0023$, μ_0 is the Bohr magneton, and $\boldsymbol{B}$ is the magnetic field vector. The total wave function is expanded in products of rotational and spin functions of the diatomic molecule and the eigenfunctions of the L^2 operator as follows:

TABLE I. Bound levels of ^{4}He–NH on potential I (in column 4) and potential II (in column 5) and of ^{3}He–NH on potential I (in column 6). All the levels correspond to the approximate quantum numbers $N=0$ and $j=1$. The approximate quantum number L, with the values indicated in column 3, is nearly conserved. Energies are relative to the ground-state energy of NH($X\ ^3\Sigma^-$), which is -0.0077 cm^{-1}. Energies in parentheses in column 4 are obtained with the spin-spin and spin-rotation interaction constants λ_0 and γ_0 set to zero.

			^{4}He–NH		^{3}He–NH
J	Parity	L	Energy (cm^{-1})	Energy (cm^{-1})	Energy (cm^{-1})
1	−	0	−4.4174(−4.4174)	−4.4266	−3.5218
0	+	1	−3.7790(−3.7818)	−3.7883	−2.7692
1	+	1	−3.7832(−3.7818)	−3.7925	−2.7727
2	+	1	−3.7815(−3.7818)	−3.7909	−2.7713
1	−	2	−2.5365(−2.5375)	−2.5462	−1.3256
2	−	2	−2.5385(−2.5375)	−2.5481	−1.3268
3	−	2	−2.5372(−2.5375)	−2.5469	−1.3260
2	+	3	−0.7536(−0.7538)	−0.7634	
3	+	3	−0.7542(−0.7538)	−0.7640	
4	+	3	−0.7537(−0.7538)	−0.7636	

$$\Psi = \sum_N \sum_{M_N} \sum_S \sum_{M_S} \sum_L \sum_{M_L} F_{NM_N SM_S LM_L}(R) Y_{NM_N}(\hat{\boldsymbol{r}}) \tau_{SM_S} Y_{LM_L}(\hat{\boldsymbol{R}}), \tag{14}$$

where M_N, M_S, and M_L denote the projections of $\boldsymbol{N}$, $\boldsymbol{S}$, and $\boldsymbol{L}$ on the magnetic field axis. In contrast with the bound state calculations in the preceding section, an uncoupled rotational and spin basis was used here, since the total angular momentum J is not conserved in the presence of an external magnetic field.

The matrix elements of the interaction potential V of Eqs. (8) and (12) in the SF basis of Eq. (14) can be evaluated by means of the Wigner–Eckart theorem.[40] They are given in Eq. (12) of Ref. 24. Also the matrix elements of the spin-spin interaction of Eq. (11) in the uncoupled SF basis have been evaluated in Ref. 24, Eq. (16). The matrix elements of the spin-rotation operator can be readily obtained using the identity

$$\gamma_0 \boldsymbol{N} \cdot \boldsymbol{S} = \gamma_0 \left[N_z S_z + \tfrac{1}{2}(N_+ S_- + N_- S_+) \right], \tag{15}$$

where $N_\pm$ and $S_\pm$ are ladder operators.[40] They are explicitly given in Eq. (13) of Ref. 24.

The Hamiltonian matrix at $R=\infty$ was diagonalized to yield the collision channels $|\alpha L M_L\rangle$. They are products of eigenfunctions of the NH monomer Hamiltonian, labeled by α, and spherical harmonics $Y_{LM_L}(\hat{\boldsymbol{R}})$. They are related to the basis of Eq. (14) by the transformation matrix $\boldsymbol{C}$, the eigenvector matrix at $R=\infty$. The scattering cross sections were then evaluated from the solution of the close coupled equations at each total energy E,

$$\left[\frac{d^2}{dR^2} - \frac{L(L+1)}{R^2} + 2\mu E \right] F_{\alpha L M_L}(R) = 2\mu \sum_{\alpha' L' M_L'} [\boldsymbol{C}^{\mathrm{T}} \boldsymbol{U} \boldsymbol{C}]_{\alpha L M_L; \alpha' L' M_L'} F_{\alpha' L' M_L'}(R). \tag{16}$$

The coupling matrix $\boldsymbol{U}$ comprises the potential energy, the NH rotational term, the spin-spin and spin-rotation interaction terms, and the Zeeman term in the basis of Eq. (14).

VI. RESULTS AND DISCUSSION

The bound energy levels of the ^{3}He–NH and ^{4}He–NH complexes computed with both potentials are listed in Table I. Energies are relative to the ground state energy of NH($X\ ^3\Sigma^-$). They agree to within about 10^{-4} cm^{-1} with the levels from the calculation in the BF Hund's case (a) representation. The intermolecular potential is weakly anisotropic, and an analysis of the energy levels and the wave functions shows that to a good approximation the SF quantum numbers N, j, and L are conserved. Since the binding energy D_0 of the complex, 4.417 and 4.427 cm^{-1} for the two potentials, is small in comparison with the rotational constant $b_{\mathrm{NH}} = 16.343$ cm^{-1}, all bound levels correspond to the ground rotational state of NH with $N=0$ and $j=S=1$. Stretch excitation is not allowed and the excited energy levels correspond to nonzero angular momentum L. There are only ten bound levels in the complex with ^{4}He and seven bound levels in the complex with ^{3}He. The ground level is characterized by $L \approx 0$, odd parity, and total angular momentum $J=1$. The excited levels of ^{4}He–NH correspond to $L \approx 1,2,3$ with an end-over-end rotational constant $B_{\mathrm{He–NH}}$ of the complex of 0.321 cm^{-1} and a distortion constant of 0.0013 cm^{-1}. The ^{3}He–NH complex with $L \approx 3$ is unbound.

The structure of the He–NH complex has been recently characterized via laser excitation of bands associated with the NH $X\ ^3\Sigma$-$A\ ^3\Pi$ transition.[41] The measurement determined the rotational constant of the ^{4}He–NH complex in the ground state to be $B_{\mathrm{He–NH}} = 0.334(2)$ cm^{-1}, in good agreement with our calculations.

In the absence of the spin-spin and spin-rotation interactions, the levels are threefold degenerate. The spin-spin and spin-rotation interactions split the levels by not more than 0.004 cm^{-1}. The levels in potential II are consistently more deeply bound than those in potential I by about 0.01 cm^{-1}. This is remarkable since the well of potential II, with $D_e = 19.80$ cm^{-1}, is slightly shallower than that of potential I with $D_e = 19.84$ cm^{-1}. It can be understood, however, since potential II is slightly more attractive than potential I for R values larger than the minimum, cf. Figs. 1 and 2, and the

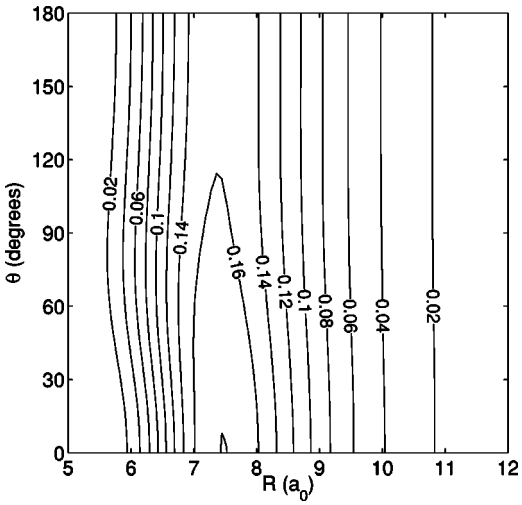

FIG. 3. Contour plot of the density distribution corresponding to the ground state with $J=1$ and $L\approx 0$. The density is obtained by integrating the square of the wave function over all coordinates except θ and R.

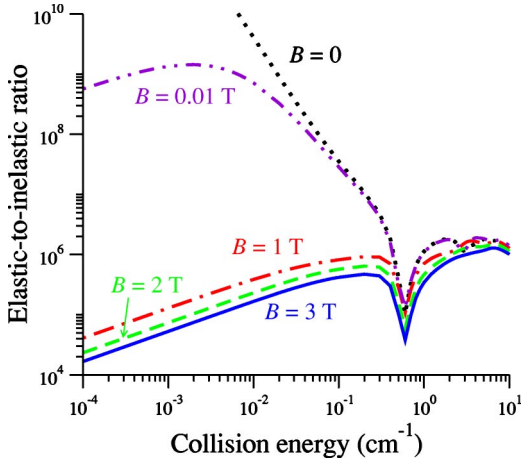

FIG. 4. Ratio of cross sections for elastic scattering and Zeeman relaxation in collisions of rotationally ground-state NH molecules with ^{3}He atoms. 1 K=0.695 cm^{-1}, note the misprint in the figure captions of Ref. 25.

bound states have their largest probability in this region, see Fig. 3. Averaging the difference potential of Fig. 1 over the density of Fig. 3 reproduces the level shift of about 0.01 cm^{-1} to within 1%. Figure 3 shows the density distribution corresponding to the ground-state wave function of ^{4}He–NH with $J=1$ and $L\approx 0$, obtained from the calculation in the BF frame. It is weakly anisotropic and has its maximum not at the minimum of the potential but at $\theta=0°$, where the potential has its lowest saddle point. The other bound states with $J=1$ ($L\approx 1,2$) and the state with $J=0$ ($L\approx 1$) have similar density distributions. The observation of scattering resonances in ^{3}He–NH cold collisions will provide a further sensitive test of the present *ab initio* calculations.

It was shown in our previous communication[25,26] that the rate constant for elastic collisions of NH with ^{3}He is much larger than the rate constant for collisionally induced Zeeman (inelastic) relaxation of NH at a temperature of 0.5 K and an external magnetic field of 100 G=0.01 T. The large values of the elastic-to-inelastic ratios indicated that the buffer-gas loading of NH will not be impeded by collisional spin depolarization. The magnetic traps of the buffer-gas loading experiments have an inhomogeneous field that varies from 0 to 4 T. In order to make definitive predictions as to the efficiency of the buffer-gas loading, an analysis of the elastic-to-inelastic ratio as a function of collision velocity and magnetic field over a wide range of these variables is needed. Figure 4 presents the ratio of rate constants for elastic scattering and Zeeman relaxation in NH–^{3}He collisions in magnetic fields from 0 to 3 T and collision energies from 10^{-4} to 1 K. The inelastic cross section was summed over both the $M_S'=0$ and $M_S'=-1$ Zeeman relaxation channels of NH($N\approx 0, S=1, M_S=1$). The elastic scattering rate constant is independent of the magnetic field. It has a magnitude of the order of 10^{-10} cm^3 s^{-1} at temperatures 0.5–1 K.

The energy transport rate constant that is usually measured in the buffer-gas cooling experiments is similar to the elastic rate constant. At 0.5 K, it is smaller than the elastic rate constant by about 30%.[25] In the limit of low temperatures, the elastic cross section is independent of the collision energy and the rate constant is proportional to $\sqrt{T}$.[42] Zeeman transitions must be accompanied by a change of the orbital angular momentum in the collision. So the Zeeman relaxation (or reorientation of the magnetic moment) cannot occur at zero temperature in the absence of a magnetic field. In a finite magnetic field, the Zeeman relaxation is an inelastic process and the Zeeman transitions are determined by the centrifugal barrier only in the incoming collision channel. Thus, the threshold behavior of the inelastic rate constant changes from $\propto T^{5/2}$ at zero magnetic field to a temperature independent constant at finite magnetic fields.[42,43] The results shown in Fig. 4 clearly reflect this behavior. The elastic-to-inelastic ratio decreases to a great extent in the vicinity of a scattering resonance (cf. Fig. 2 of Ref. 25) indicating that the inelastic cross section is much more sensitive to resonances than the elastic cross section.

In order to explore the sensitivity of the Zeeman relaxation to the interaction potential, we computed the cross sections at the magnetic field strength of 0.01 T in the energy interval between 10^{-6} and 2 cm^{-1} using both potentials. Although the potentials I and II are very similar, the Zeeman relaxation cross sections computed with potential II are larger than the cross sections obtained with potential I by as much as 40%–50% in the limit of zero collision energy. The difference becomes smaller at higher energies and is less than 10% at collision energies greater than 0.2 cm^{-1}.

We have demonstrated previously[23–25] that the mechanism driving Zeeman transitions in rotationally ground state Σ molecules depends on the spin multiplicity of the electronic state. In $^2\Sigma$ molecules[24] the coupling between the Zeeman energy levels must originate from the spin-rotation operator in Eq. (15) and there is no coupling between the Zeeman levels at very low temperature when only the ground state with $N=0$ is populated. The Zeeman transitions occur through a three-step mechanism involving rotationally excited molecular levels and the action of the spin-rotation interaction in the excited states.[23,24] The Zeeman levels in $^3\Sigma$ molecules are coupled directly by the interaction potential[24] due to the spin-spin interaction in the molecule, Eq. (11), that mixes the rotational levels with $N=0$ and $N=2$. The coupling

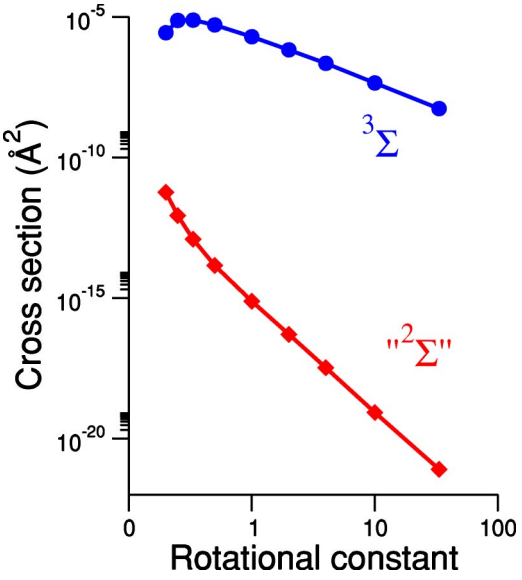

FIG. 5. Zeeman relaxation in collisions of a diatomic molecule BC with ^{3}He as a function of the rotational constant of BC. Circles, accurate calculations; squares, calculations without the spin-spin interaction. The rotational constant is given in units of b_{NH}.

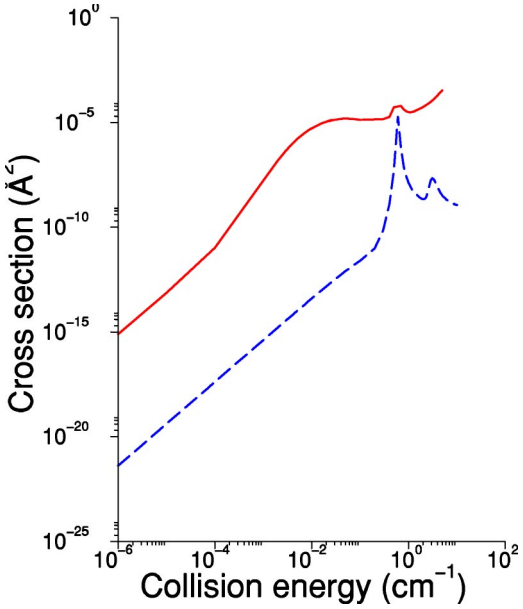

FIG. 6. Zeeman relaxation in collisions of CaH with He (solid curve) and NH with He (dashed curve) at zero magnetic field. The spin-spin interaction of NH is omitted for these calculations.

can be expressed in terms of the matrix elements of the anisotropic interaction potential, cf. Eqs. (8) and (12), connecting the $N=0$ and $N=2$ levels. The splitting between the rotational levels with different N depends on the rotational constant of the diatomic molecule and, therefore, the rate of the Zeeman relaxation in both $^2\Sigma$ and $^3\Sigma$ molecules must be sensitive to the magnitude of the rotational constant.

Figure 5 shows the dependence of the cross sections for the Zeeman relaxation in collisions of a diatomic molecule BC with ^{3}He on the rotational constant b of BC. The He–NH interaction potential and the computer program for $^3\Sigma$ molecule–He collisions were used for this calculation. The lower curve corresponds to the calculation in which the spin-spin interaction in the Hamiltonian is omitted. This omission makes the electronic state of the BC molecule to be effectively of $^2\Sigma$ molecular symmetry. The cross section is approximately proportional to $1/b^2$ for the $^3\Sigma$ molecule and to $1/b^4$ for the $^2\Sigma$ molecule, as for CaH.

It is instructive to compare the cross sections for Zeeman relaxation in CaH–^{3}He and NH–^{3}He collisions. The ground electronic state of CaH is $^2\Sigma^+$. The reduced masses of the CaH–^{3}He and NH–^{3}He complexes are similar. The equilibrium distance of CaH is $3.80a_0$ and that of NH is $1.96a_0$. As a result, the rotational constant of CaH is about 1/4 of the rotational constant of NH. Figure 6 compares the cross sections for Zeeman relaxation in CaH–^{3}He and NH–^{3}He collisions. The spin-spin interaction in NH was omitted for this calculation. The cross section for Zeeman transitions in CaH is more than five orders of magnitude larger. According to the $1/b^4$ dependence in the cross section for $^2\Sigma$ molecules the factor of $\frac{1}{4}$ in the rotational constant would suppress the cross section by a factor of 256. The fact that the actual ratio is much larger ($\approx 10^5$–10^6) is due to the different anisotropies of the He–NH and He–CaH interaction potentials. The CaH molecule is more stretched than NH and the interaction potential of the He–CaH complex is much more anisotropic than the He–NH potential. The calculation with the spin-spin interaction and a magnetic field of 100 G reveals a similar dependence of zero energy Zeeman relaxation on the interaction anisotropy: the cross section computed with the He–CaH potential is about five to six orders of magnitude larger than the cross section obtained with the He–NH potential. These tests indicate that the Zeeman relaxation in collisions of rotationally ground-state $^2\Sigma$ and $^3\Sigma$ molecules with He atoms is extremely sensitive to the anisotropy of the atom–molecule interaction potential.

VII. SUMMARY

We have completed a comprehensive study of the He–NH complex. We have generated an accurate potential for the He–NH interaction and computed bound energy levels of the complex. The effects of the molecular fine structure on the energies of the bound states have been investigated; future spectroscopic measurement of these energies will provide a sensitive test of the potential surface. A detailed study of elastic and inelastic collisions of NH with ^{3}He is presented. We have discussed the mechanisms of the Zeeman relaxation in collisions of diatomic molecules in the $^2\Sigma$ and $^3\Sigma$ states with structureless atoms such as He and analyzed the effects of external magnetic fields on the collisionally induced Zeeman relaxation in molecules. While the elastic cross section is independent of the magnetic field in the interval between 0 and 3 T, the Zeeman relaxation cross section rapidly increases with the magnetic field strength at ultralow collision energies. Both the rotational constant of the diatomic molecule and the anisotropy of the He–diatomic molecule interaction potential appear to have a strong influence on the rate constants for Zeeman relaxation. The Zeeman relaxation cross section at ultralow energies is extremely sensitive to the atom–diatomic molecule interaction

potential: a slight variation of the potential surface due to differences in fitting procedures modifies the inelastic cross section at zero energy by as much as 50%.

ACKNOWLEDGMENTS

This work was supported by NSF through grants to the Harvard-MIT Center for Ultracold Atoms and the Institute for Theoretical Atomic, Molecular and Optical Physics (ITAMP) at Harvard University and Smithsonian Astrophysical Observatory. J.K. acknowledges financial support from the European Research Training Network THEONET II and A.D. from the Chemical Sciences, Geosciences and Biosciences Division of the Office of Basic Energy Sciences, Office of Science, U.S. Department of Energy. R.V.K. was supported by the Center for Ultracold Atoms at Harvard University and Massachusetts Institute of Technology.

[1]J. Doyle, B. Friedrich, R. V. Krems, F. Masnou-Seeuws, Eur. Phys. J. D **31**, 149 (2004).
[2]C. A. Regal, M. Greiner, and D. S. Jin, Phys. Rev. Lett. **92**, 040403 (2004); C. A. Regal, C. Ticknor, J. L. Bohn, and D. S. Jin, Nature (London) **424**, 47 (2003).
[3]S. Jochim, M. Bartenstein, A. Altmeyer, G. Hendl, C. Chin, J. Hecker Denschlag, and R. Grimm, Phys. Rev. Lett. **91**, 240402 (2003).
[4]M. W. Zwierlein, C. A. Stan, C. H. Schunck, S. M. F. Raupach, S. Gupta, Z. Hadzibabic, and W. Ketterle, Phys. Rev. Lett. **91**, 250401 (2003).
[5]R. Wynar, R. S. Freeland, D. J. Han, C. Ryu, and D. J. Heinzen, Science **287**, 1016 (2000).
[6]T. Takekoshi, B. M. Patterson, and R. J. Knize, Phys. Rev. Lett. **81**, 5105 (1998).
[7]A. J. Kerman, J. M. Sage, S. Sainis, T. Bergeman, and D. DeMille,Phys. Rev. Lett. **92**, 033004 (2004).
[8]Y. B. Band and P. S. Julienne, Phys. Rev. A **51**, R4317 (1995).
[9]R. Côté and A. Dalgarno, Chem. Phys. Lett. **279**, 50 (1997).
[10]A. Fioretti, D. Comparat, A. Crubellier, O. Dulieu, F. Masnou-Seeuws, and P. Pillet, Phys. Rev. Lett. **80**, 4402 (1998).
[11]A. N. Nikolov, E. E. Eyler, X. T. Wang, J. Li, H. Wang, W. C. Stwalley, and P. L. Gould, Phys. Rev. Lett. **82**, 703 (1999).
[12]M. Gupta and D. Herschbach, J. Phys. Chem. A **103**, 10670 (1999).
[13]H. L. Bethlem, G. Berden, A. J. A. van Roij, F. M. H. Crompvoets, and G. Meijer, Phys. Rev. Lett. **84**, 5744 (2000).
[14]H. L. Bethlem, G. Berden, and G. Meijer, Phys. Rev. Lett. **83**, 1558 (1999).
[15]J. M. Doyle, B. Friedrich, J. Kim, and D. Patterson, Phys. Rev. A **52**, R2515 (1995).
[16]J. D. Weinstein, R. deCarvalho, T. Guillet, B. Friedrich, and J. M. Doyle, Nature (London) **395**, 148 (1998); J. D. Weinstein, Ph.D. thesis, Harvard University, 2001.
[17]A. Volpi and J. L. Bohn, Phys. Rev. A **65**, 064702 (2002).
[18]J. L. Bohn, Phys. Rev. A **63**, 052714 (2001).
[19]J. L. Bohn, Phys. Rev. A **62**, 032701 (2000).
[20]J. L. Bohn, Phys. Rev. A **61**, 040702 (2000).
[21]A. V. Avdeenkov and J. L. Bohn, Phys. Rev. A **64**, 052703 (2001).
[22]J. M. Doyle (private communication).
[23]R. V. Krems, A. Dalgarno, N. Balakrishnan, and G. C. Groenenboom, Phys. Rev. A **67**, 060703 (2003).
[24]R. V. Krems and A. Dalgarno, J. Chem. Phys. **120**, 2296 (2004).
[25]R. V. Krems, H. R. Sadeghpour, A. Dalgarno, D. Zgid, J. Kłos, and G. Chałasiński, Phys. Rev. A **68**, 051401 (2003).
[26]1 K = 0.695 cm^{-1}, note the misprint in the figure captions of Ref. 25.
[27]S. F. Boys and F. Bernardi, Mol. Phys. **19**, 553 (1970).
[28]MOLPRO is a package of *ab initio* programs written by H.-J. Werner and P. J. Knowles, with contributions from R. D. Amos, A. Berning, D. L. Cooper *et al.*
[29]D. Boudjaadar, J. Brion, P. Chollet, G. Guelachvili, and M. Vervloet, J. Mol. Spectrosc. **119**, 352 (1986).
[30]G. C. Groenenboom and I. M. Struniewicz, J. Chem. Phys. **113**, 9562 (2000).
[31]A. D. Esposti and H.-J. Werner, J. Chem. Phys. **93**, 3351 (1990).
[32]J. Tennyson and J. Mettes, Chem. Phys. **76**, 195 (1983).
[33]G. Jansen, B. A. Hess, and P. E. S. Wormer, Chem. Phys. Lett. **214**, 103 (1993).
[34]C. R. Brazier, R. S. Ram, and P. F. Bernath, J. Mol. Spectrosc. **120**, 381 (1986).
[35]M. Mizushima, *The Theory of Rotating Diatomic Molecules* (Wiley, New York, 1975).
[36]D. M. Brink and G. R. Satchler, *Angular Momentum* (Clarendon, Oxford, 1993).
[37]J. Tennyson and B. T. Sutcliffe, J. Chem. Phys. **77**, 4061 (1982).
[38]D. T. Colbert and W. H. Miller, J. Chem. Phys. **96**, 1982 (1992).
[39]G. C. Groenenboom and D. T. Colbert, J. Chem. Phys. **99**, 9681 (1993).
[40]R. N. Zare, *Angular Momentum* (Wiley, New York, 1988).
[41]G. Kerenskaya, U. Schnupf, M. C. Heaven, and A. van der Avoird, J. Chem. Phys. **121**, 7549 (2004).
[42]R. V. Krems and A. Dalgarno, Phys. Rev. A **67**, 050704 (2003).
[43]R. V. Krems and A. Dalgarno, Phys. Rev. A **68**, 013406 (2003).